Novel Phase Doppler Profile Sensor for Simultaneous Measurement of Size, Velocity, and Position of Droplets

Martin Niehoff[1,*], Reinhold Kneer[1], Michael Dues[2], Adi Siswanto[2], Manuel A. Reddemann[1]

1: Institute of Heat and Mass Transfer, RWTH Aachen University, Aachen, Germany
2: ILA R&D GmbH, Jülich, Germany
*Corresponding author: niehoff@wsa.rwth-aachen.de

Keywords: Interferometry, LDV, LDV-PS, Phase-Doppler technique, PDPS

ABSTRACT

In numerous technical flow applications knowing size, velocity, and position of dispersed structures simultaneously enables the comprehensive characterization of the underlying dynamics. A suitable interferometric measurement technique capable of measuring simultaneously the three droplet characteristics is introduced for the first time. This novel measurement technique called phase Doppler profile sensor (PDPS) combines the measuring principles of the laser Doppler profile sensor (LDV-PS) for velocity measurement along a measuring line with the phase Doppler technique for particle size determination. A proof-of-concept of this technique was successfully performed by comparison to another established measurement technique on a controlled use case of a displaceable mono-disperse droplet stream. In this first optical setup, a conventional phase-Doppler sensor is used as receiving unit with a conventional pinhole aperture cutting the measurement volume. Hence, the resulting performance for simultaneously measuring the droplet diameter, velocity and position along a measuring line mark the preliminary status reached and are supposed to improve in future measurements with a removed pinhole aperture. So far, the average relative deviation of PDPS compared to the reference technique simultaneously measuring diameter, position, and velocity is 1.14 % (diameter), 2.18 % (position), and 0.4 % (velocity) when using a general laboratory setup.

1. Introduction

A comprehensive characterization of the dynamics of dispersed flows requires accurate data on the size and velocity of the droplets or particles involved as a function of their position within the flow. Technical flow applications, where the simultaneous knowledge of the size, velocity, and position of dispersed structures would aid understanding are in the context of sprays and impinging jets. A prominent disperse flow is the spray cooling of electrical high-performance components (Xu et al., 2022), in which a boundary layer is formed over the surface to be cooled. Therein, droplets move with different characteristics, depending on the height above the surface (Asgari & Amani, 2021; Arcoumanis & Chang, 1994).

In many cases, these three droplet parameters are determined by separate measurements or by using complementary measurement systems based on imaging techniques as well as on interferometric techniques.

Image capture of dispersed structures also known as shadowgraphy (Hofeldt & Hanson, 1991; Bongiovanni et al., 1997) allows the measurement of a droplet diameter and position. In case at least two consecutive image frames are available, velocity measurements are possible, either by structure tracking (particle tracking velocimetry, PTV) or by cross-correlation of image areas (particle image velocimetry, PIV). Image capturing techniques like the micro particle image velocimetry (μ-PIV) can be applied even in the challenging context of micro-channels to measure the near-wall two phase flow (Lindken et al., 2009) and allow furthermore detailed flow visualization. However, image capturing techniques reach their limits because of their need for expensive computer storage and computing power for image post-processing (Kumara et al., 2010). In addition, due to the imaging to a CCD sensor of a camera with limited pixel resolution, a compromise between high spatial resolution and high spatial range must be made.

In contrast to imaging techniques, conventional interferometric methods are not capable of simultaneously detecting droplet properties of size, velocity, and position. Only by combining complementary measuring systems all three droplet parameters can be captured.

A measurement system for determining the diameter and velocity of droplets comprises the phase-Doppler technique and was initially introduced by Flögel (1981) and further investigated by Bachalo & Houser (1984); Naqwi & Durst (1991, 1992); Borys (1996) and Damaschke (2003). The technique is well explained and summarized by Albrecht et al. (2002). The phase-Doppler technique is widely applied for diameter and velocity measurements of droplets because of its fast dynamic response, high spatial resolution, wide velocity measurement range, where even reversal flows can be detected, without the computer-aided and equipment-based hurdles by image capture (Kumara et al., 2010). However, for measuring a wide spatial region, traversing the optics becomes inevitable.

An interferometric method that is capable to measure the velocity along a measuring line and thus replaces the need for traversing the optics is called the laser Doppler velocimetry profile sensor (LDV-PS). The LDV-PS is introduced by Czarske (2001); Czarske et al. (2002). The recent applications in a fuel cell micro-channel (Buerkle et al., 2020) or flow measurements in the wake of an adhering and oscillating droplet (Burgmann et al., 2021) demonstrate the LDV-PS capabilities to assist in comprehending hidden flows dynamics. However, the droplet diameter cannot be measured with the LDV-PS.

With interferometric laser Doppler techniques, the droplet properties size, velocity and position are determined with at least two separate systems. However, the use of these separate systems in a complementary measurement complicates the identification of possible physical correlations of the droplet parameters.

Against this background, a measurement system that can determine the size, velocity and position of individual droplets or particles simultaneously and without traversing the optics is of

great interest and helps comprehensively characterize the dynamics of dispersed flows. For this purpose, a laser-optical and therefore contactless measuring device has been developed, called phase-Doppler profile sensor (hereafter abbreviated as PDPS). The measurement principle of the PDPS is introduced in the following section. Thereafter, a proof-of-concept for this new measurement technique is shown as well as an evaluation considering the so far achievable accuracy in the simultaneous measurement of droplet size, velocity and position.

2. Phase Doppler profile technique

A novel phase Doppler Profile sensor is introduced enabling the simultaneous determination of size, velocity and position of individual droplets or particles without traversing of optics. This sensor combines the measuring principles of the laser Doppler profile sensor (LDA-PS) for velocity measurement along a measuring line (Czarske, 2001; Czarske et al., 2002) with the phase Doppler technique for particle size determination (Flögel, 1981; Bachalo & Houser, 1984; Bauckhage & Flögel, 1985).

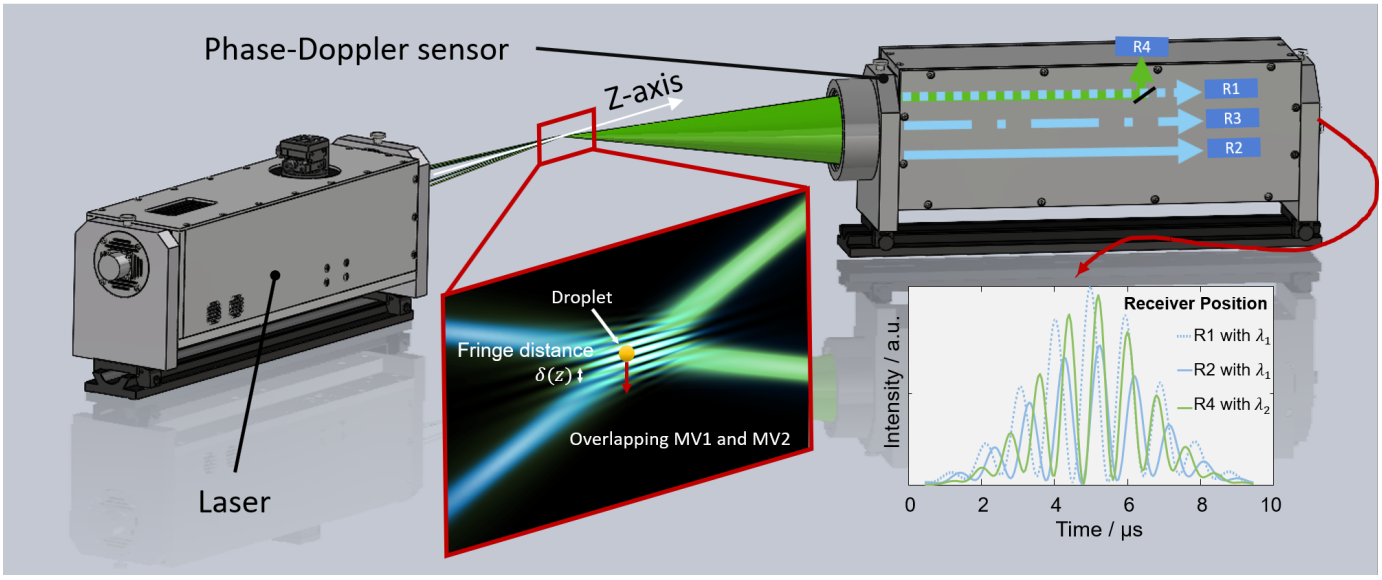

Figure 1. Principle of the PDPS technique: A converging and diverging fringe system is created. For representative causes, the depicted wavelengths do not correspond to the actual wavelengths used in the measurements. Furthermore, both the aspect ratio of the measurement volume and the angle of intersection were chosen here to exaggerate the principle for better understanding. Note that the two fringe systems have been displayed on top of each other. The blue light has the beam waists to the left of the measurement volume and converging fringe distances. For the green light it is the other way around. Droplets moving through these measurement volumes scatter the laser light with the respective wavelength to the Phase-Doppler sensor. Subsequent to the spatial segments at different elevation angles, the scattered light is received by photo-multipliers.Thereafter, the signals are processed according to their phase differences and frequencies.

In Figure 1, the set-up of PDPS is schematically depicted. Part of this sensor is the laser beam transmitter known from LDV-PS on the left side. Following the LDV-PS technique, two superimposed measurement volumes MV1 and MV2 with distinguished laser light wavelengths λ_1 and

λ_2 are created. In contrast to conventional LDV where planar fringes are used, a diverging fringe system is established in measurement volume MV1 (i.e. with increasing fringe distance $\delta_1(z)$) and in the same plane a converging fringe system in measurement volume MV2 (i.e. with decreasing fringe distance $\delta_2(z)$). Diverging or converging fringes are obtained by positioning the beam waists $\mathrm{z_{th}}$ of the two laser beams per wavelength outside the crossing points. Therefore, by consciously de-aligning the beam waist positions, the wave fronts of the laser beams in the illuminated measurement volume can not be assumed to be planar anymore. This results in either converging or diverging fringe system, as illustrated in the enlarged box in Figure 1.

A droplet or particle moving through the measurement volumes with velocity v scatters the local intensity of each wavelength λ_1 and λ_2 with the frequency $\mathrm{f_1(z)}$ and $\mathrm{f_2(z)}$. With the relation $\mathrm{q(z) = f_1/f_2 = \delta_2/\delta_1}$ and the knowledge of the quotient $\mathrm{q(z)}$, the position along the optical axis z of a particle moving through the measurement volumes can be determined by measuring the frequencies $\mathrm{f_1}$ and $\mathrm{f_2}$. A necessary requirement is that this quotient curve $\mathrm{q(z)}$ behaves monotonously preventing ambiguity in the position. The velocity then is calculated from the local fringe distance and the measured frequency as $\mathrm{v = f_1(v,z) \cdot \delta_1(z) = f_2(v,z) \cdot \delta_2(z)}$.

To measure the diameter of droplets, the LDV-PS is enhanced by the conventional phase-Doppler technique, i.e. the diameter is proportional to the measured phase difference between two receivers. The phase-Doppler sensor is shown in Figure 1 on the right side. The phase-Doppler receiver is positioned in a way that one scattering order is dominant. This necessity results from the underlying scattering theory of geometrical optics and ensures i.a. a linear relationship between phase difference and diameter.

The phase difference $\Delta\Phi^{(2)}_{\mathrm{planar}}$ between two symmetrical receivers can be described analytically according to Borys (1996) as

$$\Delta\Phi^{(2)}_{\mathrm{planar}} = d_p \cdot \beta_{\mathrm{planar}} \tag{1}$$

$$\text{with } \beta^{(2)}_{\mathrm{planar}} = \frac{2\pi}{\lambda_b}\left(\sqrt{1+\mathrm{m}^2-\mathrm{m}\sqrt{2}\sqrt{1+\sin\varphi\cos\frac{\theta}{2}+\cos\varphi\cos\vartheta\cos\frac{\theta}{2}}}\right. \tag{2}$$

$$\left.-\sqrt{1+\mathrm{m}^2-\mathrm{m}\sqrt{2}\sqrt{1-\sin\varphi\cos\frac{\theta}{2}+\cos\varphi\cos\vartheta\cos\frac{\theta}{2}}}\right) \tag{3}$$

with droplet diameter $\mathrm{d_p}$, intersection angle θ, off-axis angle ϑ, elevation angle φ, refraction index m and geometrical conversion factor β_{planar}.

In contrast to the conventional phase-Doppler technique, the wave fronts in the measurement volumes used here cannot be assumed to be planar anymore due to the conscious misalignment of the beam waist positions for a converging or diverging fringe system. This leads to Gaussian phase deviation with respect to the laser beam $b \in (1,2)$ and receiver $r \in (1,2)$ and is denoted

according to Albrecht et al. (2002) as

$$\psi_{\mathrm{G,br}} = -\mathrm{k_b}\frac{\mathrm{r_b^2}}{2\mathrm{R_b}} + \arctan\frac{\mathrm{z_b}}{\mathrm{l_R b}} \tag{4}$$

with wavefront curvature $\mathrm{R_b}$, radial spherical coordinate $\mathrm{r_b}$, Rayleigh length $\mathrm{l_{Rb}}$ and z-coordinate in the beam coordinate system $\mathrm{z_b}$.

The phase difference $\Delta\Phi_{\mathrm{meas}}$ measured with the PDPS is finally composed of the phase difference of the plane wave case $\Delta\Phi^{(2)}_{\mathrm{planar}}$ and the total phase deviation of the Gaussian beam from the plane wave case $\Delta\Phi_{\mathrm{error}}$. The magnitude of $\Delta\Phi_{\mathrm{error}}$ depends not only on the droplet position, the optical set-up of the laser beams but also on the receiver position ($\Delta\Phi_{\mathrm{error}} = (\psi_{\mathrm{G},21} - \psi_{\mathrm{G},11}) - (\psi_{\mathrm{G},22} - \psi_{\mathrm{G},12})$). In the case of non-negligible phase errors, the measured diameter $\mathrm{d_p(z)}$ can be subject to a diameter error of $\Delta d_G = \Delta\Phi_{error}/\beta^{(2)}_{\mathrm{planar}}$. For an exemplary similar optical setup with beam waist displacement $\mathrm{z_{th}}$ = -30 mm and beam waist radius $\mathrm{r_w} = 15\,\mu\mathrm{m}$, the phase error is estimated by Equation 4 to have an approximate maximum of 5 % at the edge of the measurement volume.

Table 1. PDPS Receiver Data

Receiver	Elevation angle φ [deg]	Off-axis angle ϑ [deg]
R1 ($\lambda = 532$ nm)	3.17	65
R2 ($\lambda = 532$ nm)	-3.17	65
R3 ($\lambda = 532$ nm)	0	65
R4 ($\lambda = 553$ nm)	3.17	65

In the following measurements, the characteristics of the phase-Doppler sensor are summarized in Table 1. The sensor is operated in forward scattering mode at a scattering angle of $\vartheta = 65\,\mathrm{deg}$. Scattered light of wavelength $\lambda_1 = 532\,\mathrm{nm}$ received by the PDPS is cut into three spatial segments $\mathrm{R1}$, $\mathrm{R2}$ and $\mathrm{R3}$ with fixed elevation angles $\varphi_{\mathrm{R1}}, \varphi_{\mathrm{R2}}$ and φ_{R3}. Subsequent to each segment, there is an optical path to a photo-multiplier measuring the scattered light's intensity modulation. From these signals, the required phase differences $\Delta\Phi_{\mathrm{meas}}(\mathrm{d,z})$ and frequency $\mathrm{f_1(v,z)}$ are calculated. Simultaneously, the scattered light of the second measurement volume with wavelength $\lambda_2 = 553\,\mathrm{nm}$ is received by a fourth Receiver $\mathrm{R4}$. The second frequency $\mathrm{f_2(v,z)}$ is determined from these $\mathrm{R4}$-signals.

Finally, an optical layout error of $\pm 5\,\%$ is assumed on user-set quantities in Equation 1, such as the off-axis angle ϑ and refractive index m, resulting in an estimated maximum error of $\Delta_{\mathrm{d,user}} = \pm 3.4\,\%$. This misalignment error applies to all size measurements.

3. Experimental set-up for proof-of-concept

Optical set-up and reference measurements The overall goal of this contribution is to establish a proof of concept of this phase Doppler profile technique. Hence, main interest is to demonstrate

the PDPSs capability to simultaneously and adequately measure the position, diameter and the velocity of droplets. Therefore, each droplet characteristic is measured by the PDPS as well as by a reference method and is subsequently compared. The optical setup is shown in Figure 4. The reference measurement technique consists of a long-range high-speed microscope and a droplet stream generator. In the following, the optical set-up is described in detail and its limitations are discussed.

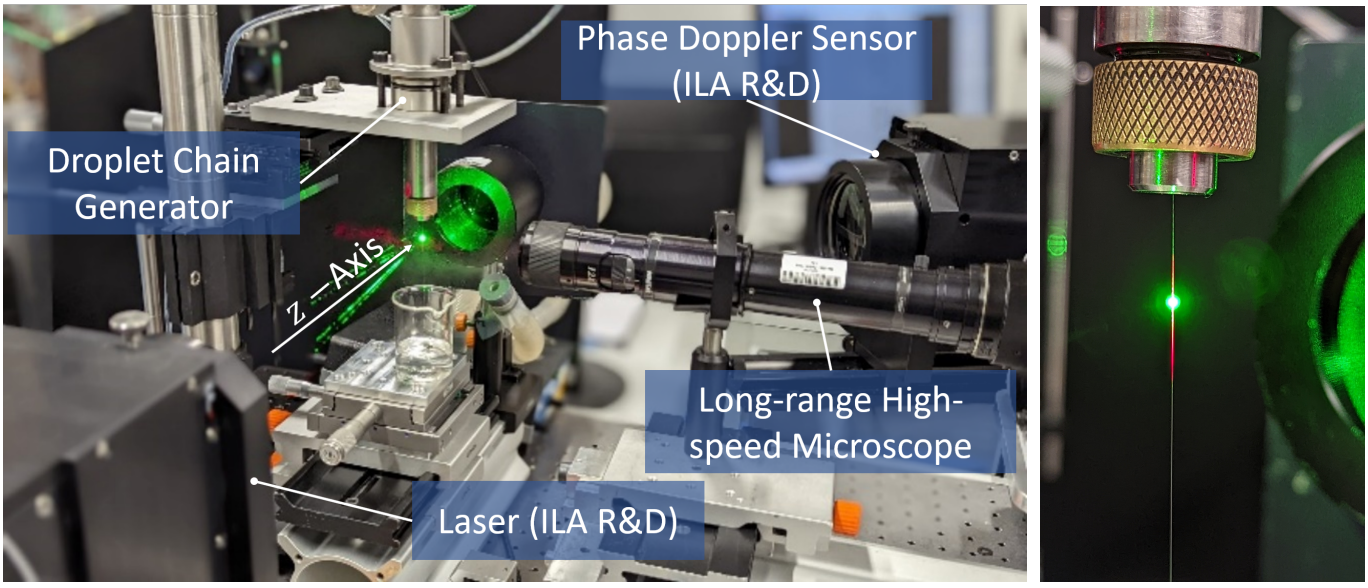

Figure 2. Left: Optical setup for comparison of the PDPS with the established HSM. Main components of the PDPS are a suitable laser and a conventional phase-Doppler sensor. Both techniques measure droplets from a mono-disperse droplet stream. Right: Close-up view of the droplet stream appearing as more or less faint vertical white line. The position illuminated by the laser beams, shows up as a bright green sphere.

Droplet stream generation A sample of droplets is required, which show a stable droplet size, position and velocity over a time frame of 0.5 s. For this purpose a mono-disperse ethanol droplet stream is used, generated by a piezoelectric droplet generator. Assuming mass conservation, the final droplet size $\mathrm{d_d}$ depends on the specific pinhole diameter of the droplet generator $\mathrm{D_{DG}}$, the applied piezoelectric frequency $\mathrm{f_{DG}}$ and the stream velocity $\mathrm{v_p}$ (Rayleigh, 1877):

$$\mathrm{d_d} = \sqrt[3]{\frac{3}{2}\frac{\mathrm{D_{DG}^2 \cdot v_p}}{\mathrm{f_{DG}}}}. \tag{5}$$

It is assumed that after each period $\mathrm{T_{DG}} = 1/\mathrm{f_{DG}}$ a droplet is dispensed in a free-fall and passes the measurement volume of the PDPS.

In this work, a frequency range of $31233\,\mathrm{Hz} < \mathrm{f_{DG}} < 31546\,\mathrm{Hz}$, pinhole diameters of $20\,\mu\mathrm{m} < \mathrm{d_{DG}} < 30\,\mu\mathrm{m}$ are used, with droplet diameters expected in the range from 49 µm to 76 µm. The position of the droplet stream flow axis is adjustable along the optical axis z via a linear stage.

Long-range high-speed microscope Simultaneous to the PDPS measurements, long-range high-speed microscope (HSM) measurements following Kirsch et al. (2019) are conducted as reference. The object plane is defined as the plane spanned by the four incident laser beams of PDPS. As high-speed camera system the Photron Fastcam SA-X with a frame rate of 40 000 fps and a resolution of 736 px 256 px is used. The high-speed camera is combined with a Navitar high magnification zoom lens. The image scale is set to 700 px/mm, which corresponds to a magnification of 14. This results in a visible range on the z-axis of 1050 µm and a depth of field of 50 µm. A Cavitar Cavilux Smart with a low degree of coherence is used as light source. It delivers almost monochromatic laser pulses at a center wavelength of $\lambda = 640\,\mathrm{nm}$ with a pulse duration of $\mathrm{t_{pulse}} = 10\,\mathrm{ns}$.

For HSM, the reliability of velocity, diameter and position measurements depends in particular on the edge localization along the pixel rows and the scale measurement error.
Due to the scale's grid width of approximate 5 px, a potential misreading of ± 5 px is expected leading to a scale measurement error of $\pm 0.712\,\%$ with respect to a scale length of 1000 µm.
With the investigated droplet size $\mathrm{d_d} > 60\,\mu\mathrm{m}$, the relative size of the projected image to the pixel size is insensitive to a droplet center being projected to center or vertex of a pixel with an average error less than 0.5 %. This error includes imperfections due to the post-processing routine, which will be introduced briefly in the following. First, for each image an adaptive threshold is calculated according to Bradley & Roth (2007). For this method, a locally adaptive threshold for each pixel using the local mean intensity around the neighbourhood of said pixel is computed. Second, each image is binarized using the aforementioned threshold method. Finally, the diameter is estimated by the following equation

$$\mathrm{d_d} = \sqrt{\frac{4 \cdot \sum \mathrm{P}}{\pi}} \cdot \frac{1}{\mathrm{s}} \tag{6}$$

with scale s and the sum of all pixel P in the region of interest. The droplet calculation in the used equation is based on a projection of a three-dimensional body and hence the assumption is made that the droplets are spherical at all times, which must not be true. These possible oscillations result in another source of error. The magnitude of this error source is not measurable in this set-up. Further possible sources of error lie in the optical set-up, since the HSM uses entocentric lenses. However, the resulting image distortion is negligible in this case.

Measurement trigger For the comparison of the two measurement techniques, identical droplets shall be recognizable by each technique. This requires perfect triggering of the two measuring systems. For this purpose, a light pulse is sent to the droplet chain, marking the start of the measurement. In Figure 3, a single expanded $532\,\mathrm{nm}$ laser pulse hits the falling droplets at the position of the measurement volume and can be recognized in the post-processing of the photo-multiplier signals as significant peak as well as in the images of HSM measurement as glare point.

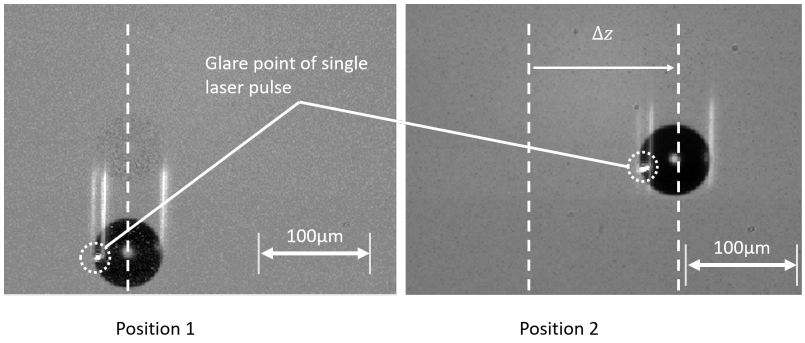

Figure 3. The mono-disperse droplet stream can be displaced in the z-axis in order to measure different droplet positions. Droplets at position 1 are observed on the left side of the image. After displacing the droplet stream by Δz, droplets can be seen at position 2 on the right side of the image. The glare point of the single laser pulse can be observed at the beginning of each measurement and marks a temporal reference. The vertical lines above the drop originate from the continuous laser light of the PDPS with the wavelength 532 nm and 553 nm. Due to the movement of the droplet and a shutter time of the camera, longer than the duration of the high-speed pulse, the glare point of the continuous laser of the falling droplet appears as a glare line.

Signal capture After the light pulse trigger has been detected, the signals from the four photo-multipliers of the PDPS are captured and stored via a Spectrum Instrumentation 14 bit digitizer (*M4i.4451-x8*) at a sampling rate of $\mathrm{F_S} = 500$ MHz. In conventional laser-Doppler measurements, neither a signal of 0.5 s length is sampled nor is the signal stored. However, this procedure is necessary with the ulterior motive of enabling a gapless recording in order to record identical droplets with both measurement techniques, beginning with the light pulse trigger. Otherwise, it cannot be guaranteed that individual droplets have not been missed. Theoretically, within the measurement time of 0.5 s approximately 15 500 droplets will be measured. A single droplet moving through the measurement volume evokes a burst signal with a specific frequency and phase. This depends on the optical set-up parameter explained above. The frequency and phase of the single bursts are calculated using a Fast Fourier Transformation. This procedure is well explained in Nobach (2001) and was implemented using MathWorks' *MATLAB* environment. The acquired signals are filtered with respect to their frequencies using a bandwidth filter from 30 MHz to 50 MHz and a minimum signal-to-noise ratio of four dB. Considering the phase-differences, the signals are filtered according to a phase tolerance usually applied in phase-Doppler measurements with 3 receivers to filter non-spherical droplets (c.f. Albrecht et al., 2002). For these PDPS measurements, $20\,\mathrm{deg}$ tolerance is accepted, corresponding to $\pm 3.4\,\mu\mathrm{m}$.

Limitations of optical set-up The main focus of these PDPS measurements is to simultaneously determine the diameter and velocity of identical droplets along a measuring line. This entails some limitations in the optical setup of this comparison.

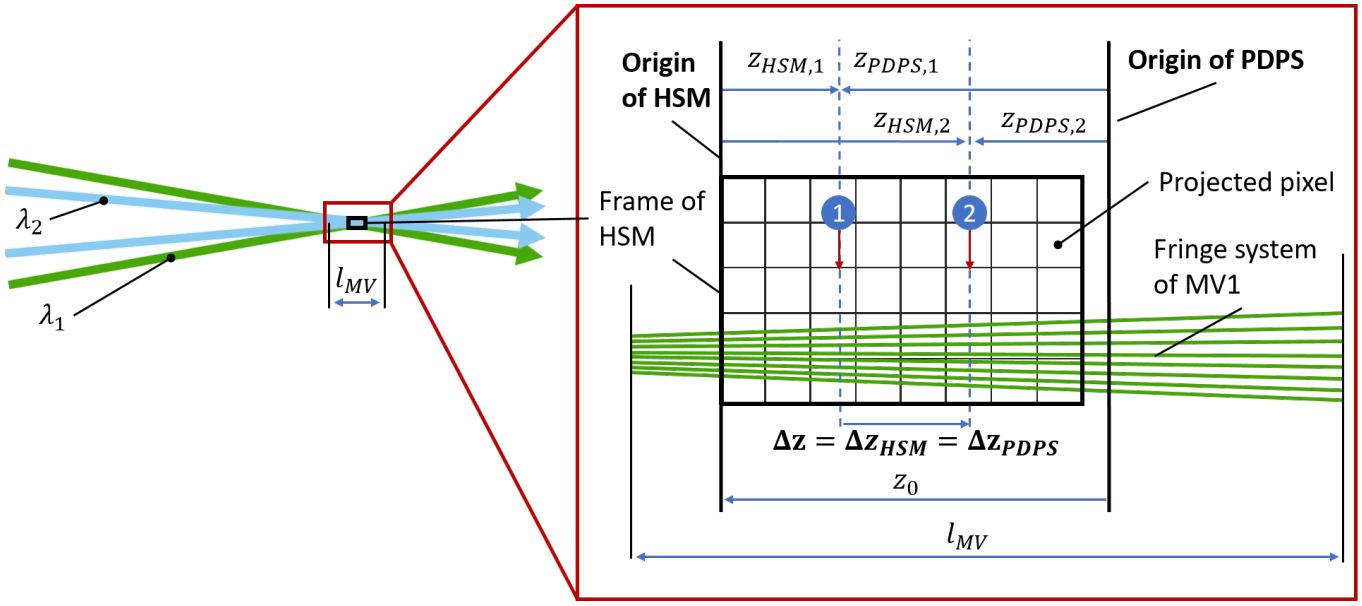

Figure 4. The relationship of coordinate system between HSM and PDPS is depicted. Left: The intersecting laser beams form a measurement volume for each wavelength. The overlapping length is shown with measurement volume length l_{MV}. The black rectangle depicts schematically the projected frame size of HSM. Right: A zoom into the rectangle is revealing the respective z-coordinates of HSM ($Z_{HSM,i}$) and PDPS ($Z_{PDPS,i}$) for two exemplary droplet stream positions $i \in (1, 2)$, displaced by $\Delta Z = \Delta Z_{HSM} = \Delta Z_{PDPS}$. A common coordinate system is obtained by subtracting z_0 from respective $Z_{HSM,i}$. A droplet at position 1 being displaced to drop position 2, equals a relative positive displacement of ΔZ_{HSM} and ΔZ_{PDPS}.

The current experimental set-up in this work provides no absolute information on the droplet position, since the coordinate origins of the HSM and PDPS are in no absolute relation to each other. In Figure 4, both coordinate systems with the respective origins are depicted. Only by ensuring that neither the measurement volume of PDPS nor the HSM system is moved relative to each other, a comparison is possible. Therefore, it must be refrained from readjustment of the laser beams or the HSM. Then, we hypothesize that a displacement of the droplet stream along the z-axis is measured equally with PDPS and HSM ($\Delta z_{HSM} = \Delta z_{PDPS}$). The figurative meaning of this hypothesis equals a slope of one in the context of linear regression and will be investigated in the next section in Figure 5b. The coordinate systems can be finally aligned by subtracting the offset z_0 from HSM measured positions z_{HSM}.

The accuracy of position, velocity and size determination of PDPS depends on the measured signal quality. The signal quality abruptly deteriorates in some cases in response to the movement of the droplet stream along the measuring line. This behavior is caused by the slit effect due to the pinhole aperture in the phase-Doppler sensor. Detailed information on the slit effect is given by Albrecht et al. (2002). The pinhole aperture is used in this very first phase-Doppler sensor version to protect the photo-multipliers from unexpected scattering or reflection. Effects due to the pinhole aperture can be avoided by moving the receiving phase-Doppler sensor in parallel along the z-axis together with the droplet stream. In future measurements the pinhole aperture will be removed. Hence, merely an intermediate accuracy will be determined and discussed in this contribution.

4. Results

In the following, sizes, velocities, and positions of droplets simultaneously measured using PDPS are compared with reference values from HSM. In this context, 24 measurements are performed, each with a different position of the droplet stream along the z-axis and different droplet sizes. First, an overview of the individual measurements is shown in Figure 5. The uncertainty of PDPS

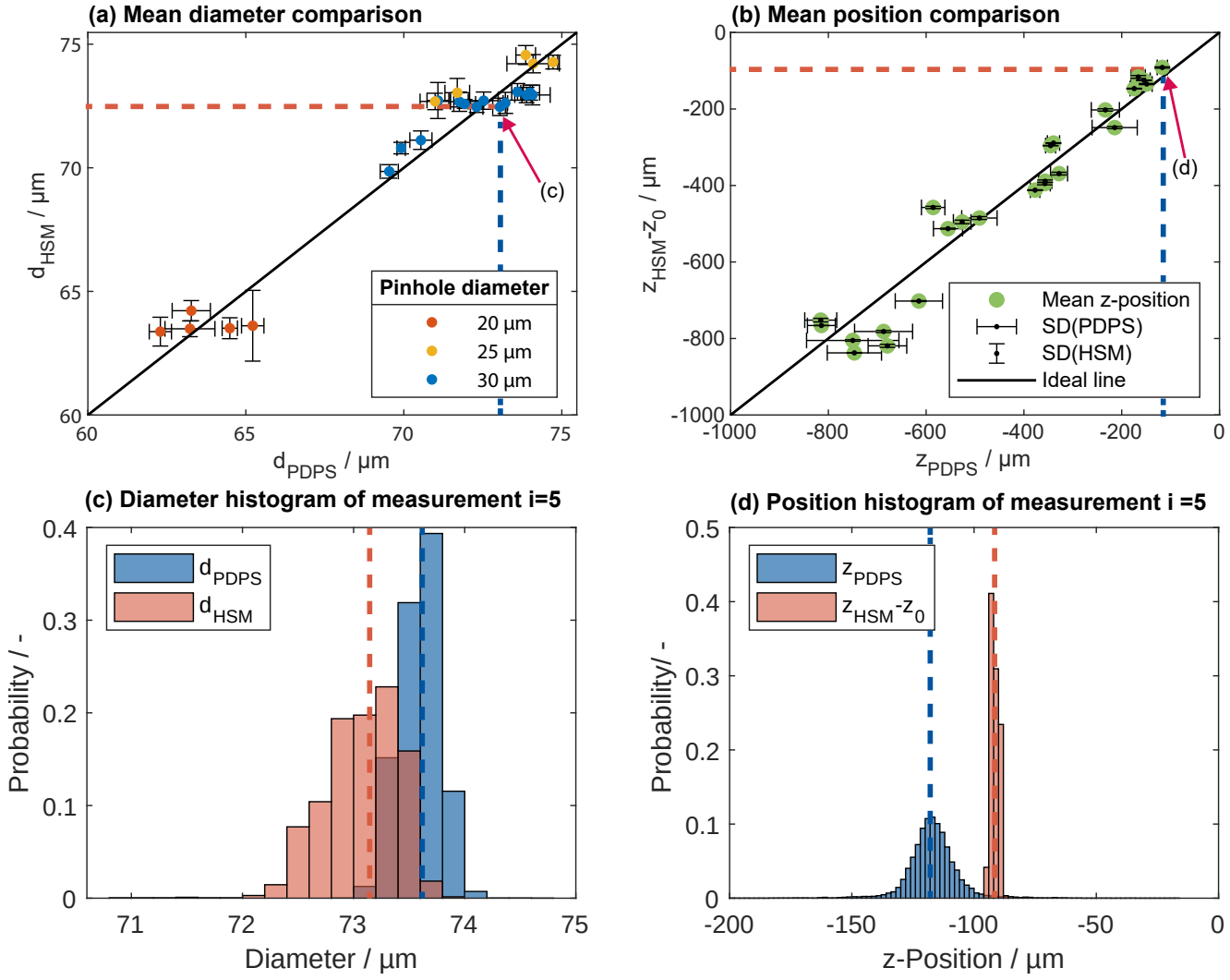

Figure 5. Figure (a) shows the mean diameters measured by PDPS d_{PDPS} versus HSM reference measurements d_{HSM} grouped by the pinhole size of the droplet chain generator D_{DG}. The black line represents the case of ideal and consistent diameter measurements of the two techniques. Vertical error bars show the SD of HSM measurements. Horizontal error bars show the SD of PDPS measurements. Figure (b) shows the comparison of droplet position along the z-axis between PDPS (z_{PDPS}) and HSM z_{HSM}-z_0, where the error bars represent the corresponding oriented SD. The SD(HSM) values are remarkably small, that's why these are almost not visible in this figure. Figures (c) and (d) show exemplary histograms of a measurement case i=21 of PDPS and HSM with respect to their measured droplet size and position. The respective average value represented by a dot in figure (a) as well as (b) can be found as a dashed line in figure (c) and (d).

measurements is evaluated in the form of standard deviations (error bars). Thereafter, the overall measurement performance with respect to velocity, size and position of PDPS is compared to the

HSM reference measurements as mean absolute deviation and mean relative deviation.

Figure 5a shows a comparison of the droplet size measured using HSM (ordinate) and PDPS (abscissa). Note that each mean droplet diameter is determined on the basis of identical droplet samples. Sampling is initiated by the trigger light pulse and ends after 0.5 s. The standard deviations of the diameter measurements are indicated by corresponding error bars parallel to the ordinate (for HSM) and to the abscissa (PDPS). Over a diameter range of 62 µm to 74 µm the measured droplet diameters with both techniques show a similar trend, i.e. HSM and PDPS show consistency in measured droplet diameters by their location near the ideal black line.

Uncertainty of PDPS The standard deviations of mean droplet diameters in Figure 5a are similar for both techniques in most cases. On average, PDPS reached a SD of diameter determination with $\bar{\sigma}_{\mathrm{d}} = 0.35\,\mu\mathrm{m}$ or 0.5 % with the respective HSM diameters as reference values. However, there are some isolated points, showing a significantly larger SD in case of HSM measurements compared to PDPS, and vice versa. Note, when applying the droplet stream generator, a reproducible droplet size is expected. Thus, any variance in the droplet size can be attributed to errors of the respective measurement technique, e.g. caused by frame-to-frame variation of the illumination or the droplet chain swinging perpendicular to the object plane. Further note that the evaluation algorithm of HSM measurements has difficulties determining the correct size of out of focus droplets, since the droplet edge is inaccurately localized. In contrast, PDPS either does not measure these droplets because they are then outside the measurement volume, or it measures the scattered light of a wrong scattering order, resulting in a significantly erroneous droplet size.

Figure 5b shows a comparison of the droplet position measured with PDPS (abscissa) and HSM (ordinate). For representation purposes, the two coordinate systems of PDPS and HSM are referenced to one coordinate system by zero shifting the axis intercept of the ordinate z_0, as already depicted in Figure 4. The zero offset z_0 of $1056\,\mu\mathrm{m}$ results from conducting a linear regression with a forced slope of 1 with respect to the measured cases. By forcing the slope to one, we hypothesize that HSM and PDPS measure the same positional shift in droplet stream. The hypothesis of this linear regression is valid because with the 24 cases measured, an R^2 of 0.946 and a p-value close to zero (< 5 %) are obtained. In Figure 5b, the droplet stream was obviously positioned in the left half of the PDPS measurement volume, which is defined for a measurement volume length of $\mathrm{l}_{\mathrm{MV}} = 2.376\,\mathrm{mm}$ with feasible z-positions between -1.2 mm and 1.176 mm. In contrast to this, the visible range of the HSM is limited to $1050\,\mu m$. Thus, the length available for comparison is limited by the HSM and not by the PDPS.

The error bars in Figure 5b correspond to the standard deviations when measuring the z-position with the respective measurement method. Obviously, the vertical SDs of HSM (with $\bar{\sigma}_{\mathrm{z}} = 2\,\mu\mathrm{m}$ on average, maximum $\sigma_{\mathrm{z,max}} = 9\,\mu\mathrm{m}$) are significantly lower compared to those of PDPS (with $\bar{\sigma}_{\mathrm{z}} = 28\,\mu\mathrm{m}$ on average, maximum $\sigma_{\mathrm{z,max}} = 94\,\mu\mathrm{m}$). A relative SD is obtained by referencing the SD to the measurement volume length. The mean relative SD amounts to 1.18 %, the maximal observed relative SD is 3.98 %. Thus, a significantly higher uncertainty of PDPS measurements

compared to reference measurements is observed.

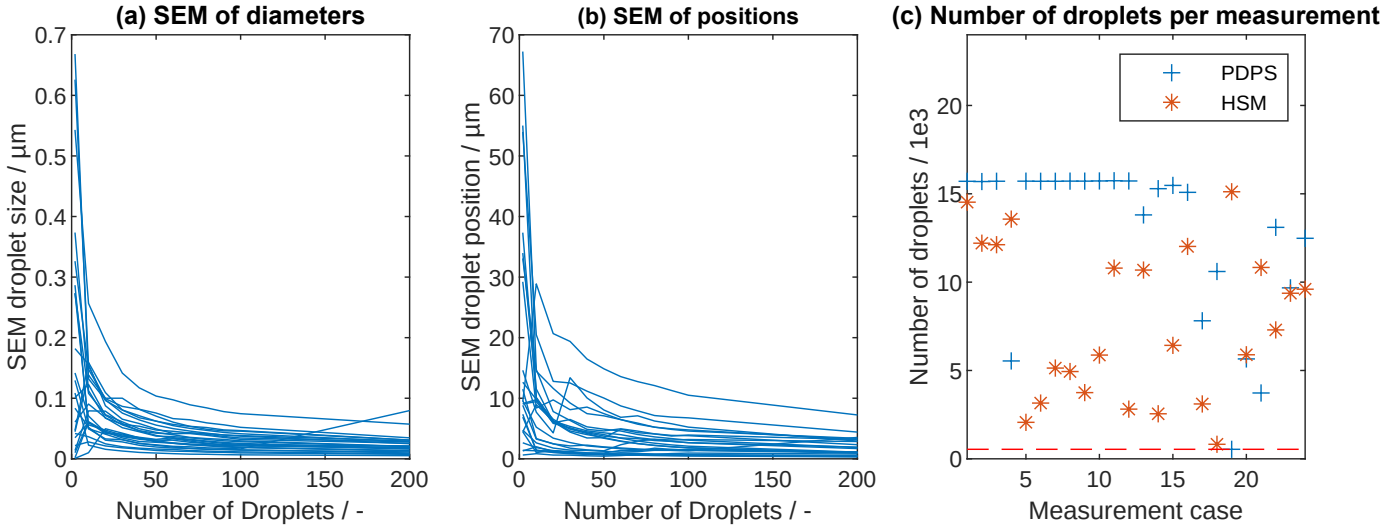

Figure 6. Left and middle: Each line represents the standard error to the mean (SEM) of the conducted diameter and position measurement with respect to the number of measured valid droplets. The SEM of the diameter and position show convergence with at least 100 droplets. Right: The number of measured droplets with both techniques is always above 500 of approximately 15 000 possibly measurable droplets. These numbers include merely actually detected droplets with HSM and droplets filtered according the signal quality criteria of PDPS.

Figure 6a and Figure 6b provide an overview of how the standard error to the mean diameter and mean position of PDPS depends on the number of measured droplets that meet the signal quality criteria of PDPS (blue) and are detected by the HSM (red) post-processing algorithm. The standard error of the mean (SEM) in the most cases shows no significant deviation if more than 100 droplets are measured. Figure 6c shows the number of evaluated droplets per measurement that fulfill the above mentioned signal criteria. As at least 500 droplets have been measured (with most cases showing more than 5000 droplets measured) in each case considered, it can be concluded from Figures 6a and 6b that the measurements can be considered statistically reliable.

Deviation of PDPS to HSM The comparison of the significantly smaller standard deviation in the position determination of the HSM to the significantly larger standard deviation of PDPS justifies using the HSM measurements as a reference. Although HSM measures with a low uncertainty, HSM itself is limited by its inherent errors due to pixel size, magnification and the applied scale. These uncertainties are not considered quantitatively in this contribution, but should be kept in mind for these comparisons.

In Figure 7a and Figure 7b, the relative deviation of PDPS to the reference is shown for simultaneously determining the size, position and velocity. The relative deviations are denoted as

$$\Delta_\mathrm{v} = \frac{\mathrm{v_{PDPS}} - \mathrm{v_{HSM}}}{\mathrm{v_{HSM}}} \qquad \Delta_\mathrm{d} = \frac{\mathrm{d_{PDPS}} - \mathrm{d_{HSM}}}{\mathrm{d_{HSM}}} \qquad \Delta_\mathrm{z} = \frac{\mathrm{z_{PDPS}} - (\mathrm{z_{HSM}} - \mathrm{z_0})}{\mathrm{l_{MV}}}. \tag{7}$$

In Figure 7a, the relative deviation of diameter determination Δ_d is compared to the relative deviation of velocity determination Δ_v. In Figure 7b, the relative deviation of size determination Δ_d

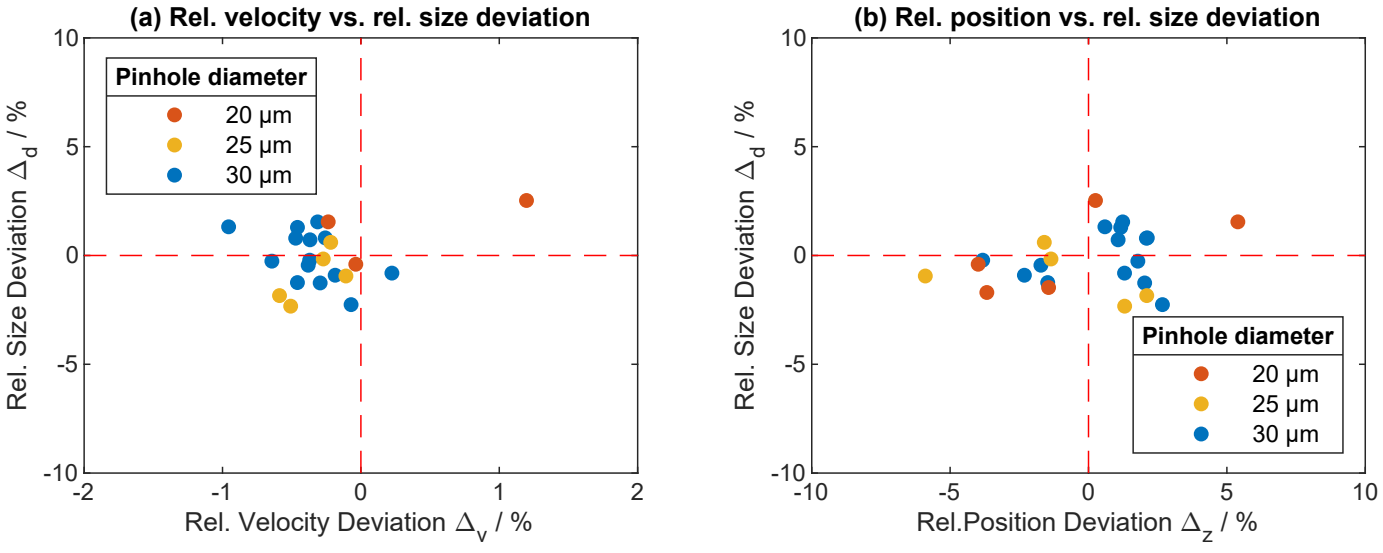

Figure 7. The relative deviation of PDPS to HSM in simultaneous measurement of size, velocity and position is shown, considering different pinhole diameters of the droplet stream generator. Left: The relative deviation of diameter determination Δ_d is compared to the relative deviation of velocity determination Δ_v. Right: the relative deviation of size determination Δ_d is compared to the relative deviation of position determination Δ_z. The red dashed lined represent the line of zero deviation.

is compared to the relative deviation of position determination Δ_z. To critically characterize the mean deviation of PDPS compared to the reference technique, the absolute mean value of the relative deviations with respect to velocity v, size d, and position z are calculated, as exemplified here for the absolute mean value of diameter determination $|\bar{\Delta}_\mathrm{d}| = \sum_{\mathrm{i=1}}^{\mathrm{n=24}} |\Delta_\mathrm{z}|/24$.

Regarding the droplet size, the mean relative deviation of PDPS and HSM amounts to $|\bar{\Delta}_\mathrm{d}| = 1.14\,\%$ which corresponds to an average absolute sizing deviation of $0.8\,\mu\mathrm{m}$. Individual relative deviations in size depicted as dots in Figure 7a can be as large as $2.53\,\%$ ($\Delta\mathrm{d}_\mathrm{d} = 1.7\,\mu\mathrm{m}$). With PDPS measurement, systematic errors can occur due to misalignment, a user-selected incorrect refractive index value, phase tolerances to filter non-spherical droplets or a position dependent Gaussian phase error. A clear position dependent superposition of these size errors cannot be observed in the data, but smaller errors may still be included or mutually cancel each other out. Detailed light-droplet interaction simulations with light scattering theories like Generalized Lorenz-Mie Theories (Gouesbet & Gréhan, 2011) could support precisely estimating the phase errors resp. size errors in the future.

Considering the droplet position, the mean relative deviation measured by PDPS compared to HSM as reference amounts to $|\bar{\Delta}_\mathrm{z}| = 2.18\,\%$ which corresponds to an average absolute position deviation of $52\,\mu\mathrm{m}$ at a measurement volume length of 2.376 mm. Individual relative deviations in position depicted as dots in Figure 7b can be as large as $5.9\,\%$, i.e. for single unfavorable measurements in Figure 5b the droplet position determined by PDPS and HSM differs by up to 140 µm.

Regarding the droplet velocity determination, the mean relative deviation of PDPS amounts to

$|\bar{\Delta}_\mathrm{v}| = 0.4\,\%$. The velocity lies in the range of $6.2784\,\mathrm{ms}^{-1}$ to $9.9866\,\mathrm{ms}^{-1}$ with SDs in the range of $0.0041\,\mathrm{ms}^{-1}$ to $0.0964\,\mathrm{ms}^{-1}$. Individual relative deviations in velocity depicted as dots in Figure 7a can be as large as $1.2\,\%$.

With PDPS not only the velocity, but also the position determination depends on the determined frequencies. As denoted above, the z-position is determined by calculating the quotient of frequencies f_1 and f_2 and matching this to the quotient $\mathrm{q(z)}$, which is determined beforehand in a calibration process. This calibration process is exemplarily described in Burgmann et al. (2021). As measure of the possible uncertainties of position determination, Büttner (2004) denotes the uncertainty according to an error propagation analysis as

$$\Delta \mathrm{z} \approx 2 \cdot \left\| \frac{\partial \mathrm{q(z)}}{\partial \mathrm{z}} \right\|^{-1} \cdot \frac{\Delta \mathrm{f}}{\mathrm{f}}. \tag{8}$$

In this work, the quotient $\mathrm{q(z)}$ has a gradient of $\partial \mathrm{q(z)}/\partial \mathrm{z} \approx 0.02679\,\mathrm{mm}^{-1}$ in the center of the measurement volume. Furthermore, assuming the uncertainty of frequency measurements $\Delta \mathrm{f}/\mathrm{f}$ to be approx. 0.4 %, a mean uncertainty of position measurements is estimated as $\Delta \mathrm{z} = 29.9\,\mu\mathrm{m}$. This quick sanity check agrees with the measurement results, since the mean SD of position determination amounts to 28 µm. This again underlines the importance of frequency determination and signal quality. Since the pinhole aperture in the phase-Doppler sensor seemed to challenge the signal quality in some cases, the pinhole shall be removed with respect to future measurements. This approach could further improve the overall performance of the PDPS.

5. Conclusion

In numerous technical flow applications the simultaneous knowledge of size, velocity, and position of dispersed structures could enable the comprehensive characterization of the underlying dynamics. In this contribution, a suitable interferometric measurement technique capable of measuring simultaneously the three droplet characteristics is introduced for the first time. This novel measurement technique called phase Doppler profile sensor (PDPS) combines the measuring principles of the laser Doppler profile sensor (LDA-PS) for velocity measurement along a measuring line with the phase Doppler technique for particle size determination. A proof-of-concept of this technique was successfully conducted by comparison to another established measurement technique on a controlled use case of a mono-disperse droplet chain. In the conducted comparison, 24 measurements of a droplet stream providing a diameter range from 62 µm to 74 µm, at different streamwise positions are performed.

On average, the relative deviation of droplet diameters measured by PDPS compared to a long-range high-speed microscope (HSM) as reference amounts to 1.14 % with an average uncertainty of 0.5 %. Considering the droplet position, the mean relative deviation measured by PDPS compared to HSM as reference is 2.18 % with an average uncertainty of 1.18 %. The relative deviation and relative uncertainty are obtained by referencing to the measurement volume length of 2.376 mm.

The velocity of the droplet stream is determined with a mean relative deviation of $0.4\,\%$ with individual relative velocity deviations below $1.2\,\%$ at a velocity range from approximately $6.3\,\mathrm{ms}^{-1}$ to $9.9\,\mathrm{ms}^{-1}$. Again, the relative deviation and uncertainty are obtained by referencing to HSM measurements. Although no clear influence of the presumed phase error due to deviation from the planar wavefront could be established with the conducted measurements, further work must be expended to quantify this error more precisely with respect to the present optical setup. The next step is to remove the pinhole aperture in the phase Doppler sensor, as this still limits the full applicability of this new technique. This will presumably improve the overall performance reached so far. This is due to the suspicion that in some of the conducted measurements the pinhole aperture has caused a slit effect or at least disturbed the received scattered light and reduced the signal quality. Furthermore, the PDPS will be applied in future measurements to more challenging and realistic test cases with a relevant range of droplets sizes and steep velocity gradients, as typically found in spray applications.

Acknowledgements

This Project (16KN042152) is supported by the Federal Ministry for Economic Affairs and Climate Action (BMWK) on the basis of a decision by the German Bundestag.

Nomenclature

CCD	charge-coupled device
HSM	Long-range High-speed Microscopy
LDV	Laser Doppler velocimetry
LDV-PS	laser Doppler velocimetry profile sensor
MV	measurement volume
PIV	particle image velocimetry
µ-PIV	micro particle image velocimetry
PDPS	phase Doppler profile sensor
PTV	particle tracking velocimetry
SD	standard deviation
SEM	standard error to the mean

β	geometrical conversion factor [$\mathrm{deg\,\mu m}^{-1}$]
δ	fringe distance [µm]
$\Delta\Phi$	phase difference [deg]
$\Delta\mathrm{Z}_{\mathrm{HSM}}$	droplet stream displacement measured by HSM [µm]
$\Delta\mathrm{Z}_{\mathrm{PDPS}}$	droplet stream displacement measured by PDPS [µm]
Δ_{d}	relative error of diameter determination [%]

Δ_v	relative error of velocity determination [%]
Δ_z	relative error of position determination [%]
λ	wavelength [nm]
θ	intersection angle [deg]
φ	elevation angle [deg]
ϑ	off-axis angle [deg]
σ	standard deviation [µm]
D_{DG}	Pinhole diameter of droplet stream generator [µm]
d_d	droplet diameter [µm]
f	Doppler burst frequency [Hz]
f_{DG}	Piezoelectric frequency [Hz]
F_s	sampling frequency [Hz]
i	measurement case
l_{MV}	length of overlapping measurement volumes [mm]
m	refractive index [-]
P	pixel in the region of interest [px]
R_b	wavefront curvature [m]
r_b	radial spherical coordinate
r_w	beam waist radius [µm]
R1	receiver 1
R2	receiver 2
R3	receiver 3
R4	receiver 4
s	scale [$\mathrm{px\,mm^{-1}}$]
v	velocity [$\mathrm{m\,s^{-1}}$]
z_0	position off-set between HSM and PDPS [µm]
z_b	z-coordiante in beam coordiante system [µm]
z_{th}	beam waist displacement [mm]

References

Albrecht, H.-E., Damaschke, N., Borys, M., & Tropea, C. (2002). *Laser doppler and phase doppler measurement techniques*. Springer Science & Business Media.

Arcoumanis, C., & Chang, J. (1994). Flow and heat transfer characteristics of impinging transient diesel sprays. *SAE transactions*, 1092–1116.

Asgari, B., & Amani, E. (2021). An improved spray-wall interaction model for eulerian-lagrangian simulation of liquid sprays. *International Journal of Multiphase Flow*, *134*, 103487.

Bachalo, W., & Houser, M. (1984). Phase/doppler spray analyzer for simultaneous measurements of drop size and velocity distributions. *Optical Engineering*, *23*(5), 235583.

Bauckhage, K., & Flögel, H. h. H. (1985). Simultaneous measurement of droplet size and velocity in nozzle sprays. In *2nd international symposium on applications of laser anemometry to fluid mechanics* (pp. 18–1).

Bongiovanni, C., Chevaillier, J. P., & Fabre, J. (1997). Sizing of bubbles by incoherent imaging: defocus bias. *Experiments in fluids*, *23*(3), 209–216.

Borys, M. (1996). *Analyse des amplituden-und phasenverhaltens von laser-doppler-signalen zur größenbestimmung sphärischer teilchen*. Shaker.

Bradley, D., & Roth, G. (2007). Adaptive thresholding using the integral image. *Journal of graphics tools*, *12*(2), 13–21.

Buerkle, F., Moyon, F., Feierabend, L., Wartmann, J., Heinzel, A., Czarske, J., & Buettner, L. (2020). Investigation and equalisation of the flow distribution in a fuel cell stack. *Journal of Power Sources*, *448*, 227546.

Burgmann, S., Dues, M., Barwari, B., Steinbock, J., Büttner, L., Czarske, J., & Janoske, U. (2021). Flow measurements in the wake of an adhering and oscillating droplet using laser-doppler velocity profile sensor. *Experiments in Fluids*, *62*(3), 1–16.

Büttner, L. (2004). *Untersuchung neuartiger laser-doppler-verfahren zur hochauflösenden geschwindigkeitsmessung*. Cuvillier Verlag.

Czarske, J. (2001). Laser doppler velocity profile sensor using a chromatic coding. *Measurement Science and Technology*, *12*(1), 52.

Czarske, J., Büttner, L., Razik, T., & Müller, H. (2002). Boundary layer velocity measurements by a laser doppler profile sensor with micrometre spatial resolution. *Measurement Science and Technology*, *13*(12), 1979.

Damaschke, N. (2003). *Light scattering theories and their use for single particle characterization*. Shaker Verlag.

Flögel, H. (1981). Untersuchung von teilchengeschwindigkeit und teilchengröße mit einem laser-doppler-anemometer. *Universität Bremen, Bremen, Germany.(See p. 33)*.

Gouesbet, G., & Gréhan, G. (2011). *Generalized lorenz-mie theories* (Vol. 31). Springer.

Hofeldt, D., & Hanson, R. K. (1991). Instantaneous imaging of particle size and spatial distribution in two-phase flows. *Applied optics*, *30*(33), 4936–4948.

Kirsch, V., Hermans, M., Schönberger, J., Ruoff, I., Willmann, M., Reisgen, U., … Reddemann, M. A. (2019). Transparent high-pressure nozzles for visualization of nozzle internal and external flow phenomena. *Review of Scientific Instruments*, *90*(3), 033702.

Kumara, W., Elseth, G., Halvorsen, B., & Melaaen, M. (2010). Comparison of particle image velocimetry and laser doppler anemometry measurement methods applied to the oil–water flow in horizontal pipe. *Flow measurement and Instrumentation*, *21*(2), 105–117.

Lindken, R., Rossi, M., Große, S., & Westerweel, J. (2009). Micro-particle image velocimetry (μpiv): recent developments, applications, and guidelines. *Lab on a Chip*, *9*(17), 2551–2567.

Naqwi, A. A., & Durst, F. (1991). Light scattering applied to lda and pda measurements. part 1: Theory and numerical treatments. *Particle & particle systems characterization*, *8*(1-4), 245–258.

Naqwi, A. A., & Durst, F. (1992). Light scattering applied to lda and pda measurements part 2: computational results and their discussion. *Particle & particle systems characterization*, *9*(1-4), 66–80.

Nobach, H. (2001). Analysis of dual-burst laser doppler signals. *Measurement Science and Technology*, *13*(1), 33.

Rayleigh, J. (1877). *The theory of sound, macmillan and co.* London.

Xu, R., Wang, G., & Jiang, P. (2022). Spray cooling on enhanced surfaces: A review of the progress and mechanisms. *Journal of Electronic Packaging*, *144*(1).